### **CONFERENCE PRE-PRINT**

# EVALUATION OF PLASMA PERFORMANCE IN JA DEMO STEADY-STATE OPERATION

S. SUGIYAMA

National Institutes for Quantum Science and Technology (QST)

Rokkasho, Japan

Email: sugiyama.shota@qst.go.jp

N. AIBA

National Institutes for Quantum Science and Technology (QST)

Naka, Japan

M. HONDA

**Kyoto University** 

Kyoto, Japan

N. ASAKURA, N. HAYASHI

National Institutes for Quantum Science and Technology (QST)

Naka, Japan

Y. SAKAMOTO, JOINT SPECIAL DESIGN TEAM FOR FUSION DEMO

National Institutes for Quantum Science and Technology (QST)

Rokkasho, Japan

#### **Abstract**

Plasma performance in steady-state operation has been evaluated by conducting integrated modelling simulations to address the uncertainties of modelling and assumptions in JA DEMO, a design concept of the steady-state tokamak demonstration reactor. The results of the integrated modelling simulations are compared to those of the systems analysis. The dependence of the plasma performance on the selection of the turbulent thermal transport model, heating and current drive conditions, and density peaking factor is investigated. The Bohm-gyroBohm, CDBM, and Coppi-Tang models predict similar plasma performance for JA DEMO conditions, while they evaluate the different temperature and current profiles. The optimal heating and current drive condition is discussed in terms of the balance between the neutral beam injection power and electron cyclotron (EC) wave injection power to maximize the non-inductive current drive fraction and the location of the EC current drive to increase the plasma performance. The high density peaking factor is preferable for the core plasma operation condition because the higher fusion power and non-inductive current drive fraction can be obtained with the lower external input power and confinement enhancement factor. Within the simulation conditions in the study, the plasma performance required for the JA DEMO steady-state operation can be sufficiently obtained.

#### 1. INTRODUCTION

The conceptual design activity for a steady-state tokamak demonstration reactor, JA DEMO [1, 2], has been conducted in Japan. The main parameters of JA DEMO are the plasma major radius of 8.5 m, minor radius of 2.42 m, plasma current of 12.3 MA, toroidal magnetic field at the plasma centre of 5.94 T, and fusion power of 1.5 GW. The plasma operation is limited by the specifications of engineering components, including the heating and current drive systems and allowable heat flux to the plasma-facing components. The plasma operation scenario development is necessary to construct a feasible DEMO concept and to determine the component designs, such as the heating and current drive systems. Previously, ohmic plasma initiation with poloidal field coil supply voltage similar to ITER [3], flux consumption reduction during plasma current ramp-up phase by electron cyclotron (EC) heating [4], external heating power required for the L–H transition [5], and fusion power control by pellet injection [6] have been studied for JA DEMO. The previous study on the steady-state plasma operation scenario from the ramp-up to the flat-top burn phases for JA DEMO evaluated the external input power required for full non-inductive current drive and pointed out the importance of off-axis EC current drive for controlling the internal transport barriers (ITBs) [2].

The two-hour pulsed plasma operation scenario has been developed for commissioning and early demonstration of power generation with lower plasma performance than that for the steady-state operation, clarifying controls of the current profile and power required for the pulsed operation [7]. These studies have identified possible plasma operation and specifications of engineering components required for plasma operation. For EU DEMO, identification of the requirements for actuators [8] and the limiter design for first wall protection [9] have been studied based on the developed plasma operation scenario and control simulations [10, 11].

To ensure that the plasma performance required for the achievement of DEMO goals is obtained, the plasma scenario should be developed based on the analyses within a wide range of assumptions, considering the modelling uncertainties. The ITER plasma performance has been compared for different turbulent thermal transport models, densities, heating and current drive schemes, and impurity concentrations [12–14]. The dependence of the plasma performance on the turbulent transport model has been examined for EU DEMO [15]. The plasma required for JA DEMO has the characteristics of a larger size and higher performance compared to the ITER plasmas and the fully non-inductive current drive, i.e., the higher non-inductive current drive fraction compared to EU DEMO which supposes no external current drive in the flat-top burn phase.

In this paper, we have evaluated the plasma performance in the JA DEMO steady-state operation by conducting integrated modelling simulations. We compare the results of the integrated modelling simulations to those of the systems analysis [2]. We investigate the dependence of the plasma performance on the selection of the turbulent thermal transport model, heating and current drive conditions, and density profile. The examined transport models predict similar values of the main parameters, whereas they evaluate the different temperature and current profiles. The optimal balance between the neutral beam injection (NBI) power and EC injection power and the optimal position of the EC current drive for ITB sustainment are discussed. The high density peaking factor is preferable to obtain the high plasma performance.

### 2. ANALYSIS MODEL

The plasma performance is evaluated using the integrated modelling code GOTRESS+ [16] which consists of the ACCOME [17], EC-Hamamatsu [18], GOTRESS [19], and OFMC [20] codes. One of the characteristics of GOTRESS+ is to find the steady-state solution directly; therefore, the code is effective for the purpose of this study. The magnetic equilibrium and bootstrap current are calculated using ACCOME. The EC-driven current and heating profiles are calculated using EC-Hamamatsu. The profiles of the current and heating by NBI are calculated using OFMC. The electron and ion temperature profiles are calculated using GOTRESS, prescribing the electron density profile and ion density fractions. The temperature profile is given in the region of  $\rho \geq 0.85$  by the hyperbolic tangent function and is solved in the core region ( $\rho < 0.85$ ). Here,  $\rho$  is the normalized minor radius. Electron, deuteron, triton, and argon (Ar) are considered in the simulation. Argon is considered as the impurity species that is injected intentionally to suppress the net plasma loss power across the separatrix,  $P_{\rm sep}$ .

The Bohm-gyroBohm (BgB) [21–23], CDBM [24, 25], and Coppi-Tang (CT) [26] models are used for the turbulent thermal transport models in this study. The formation and sustainment of ITBs are considered using the BgB model by multiplying the Bohm term by a shear function. The BgB and CDBM models well reproduce internal transport barriers (ITBs) [23] which are supposed to be utilized in the JA DEMO steady-state plasma operation [2]. The CT model has often been used for the ITER scenario studies [13, 14].

The pedestal density,  $n_{\rm ped}$ , and temperature,  $T_{\rm ped}$ , are prescribed in this study, whereas the EPED1 model [27] is implemented in GOTRESS+. We assume  $T_{\rm ped}=3$  keV for both electron and ion. We use  $n_{\rm ped}/n_{\rm GW}=0.85$  as a typical value, where  $n_{\rm GW}$  is the Greenwald density limit. It was previously confirmed that the typical values ( $n_{\rm ped}/n_{\rm GW}=0.85$  and  $T_{\rm ped}=3$  keV) are within the MHD stable region [5] using the ideal MHD stability code MARG2D [28].

The NBI system is assumed to consist of three deuterium beam injectors based on negative-ion sources. The port-through power, beam energy, and tangent radius of injection are 33 MW, 1.5 MeV, and 8.5 m, respectively. The three NBI ports are tilted downward with different angles to obtain a wider NBI-driven current profile. We assume that all EC waves are injected from a single common position with the frequency of 190 GHz and the injection angles of 30° and 0° in the toroidal and poloidal directions, respectively, to drive the current locally. Figure 1 shows the last closed flux surface and injection directions of NBI and EC waves in the (a) poloidal plane and (b) horizontal plane of the height of the magnetic axis.

#### 3. RESULTS AND DISCUSSION

Table 1 shows the values of main parameters calculated using a systems code (TPC) [2] and GOTRESS+ with the BgB, CDBM, and CT models. Here,  $P_{\rm fus}$  is the fusion power,  $P_{\rm NBI}$  is the NBI power,  $P_{\rm EC}$  is the EC injection power,  $Q = P_{\rm fus}/P_{\rm aux}$ ,  $P_{\rm aux} = P_{\rm NBI} + P_{\rm EC}$  is the total external input power,  $f_{\rm GW}$  is the line-averaged electron density normalized by the Greenwald density limit,  $\beta_{\rm N}$  is the normalized beta,  $H_{\rm H}$  is the confinement enhancement factor defined as the energy confinement time

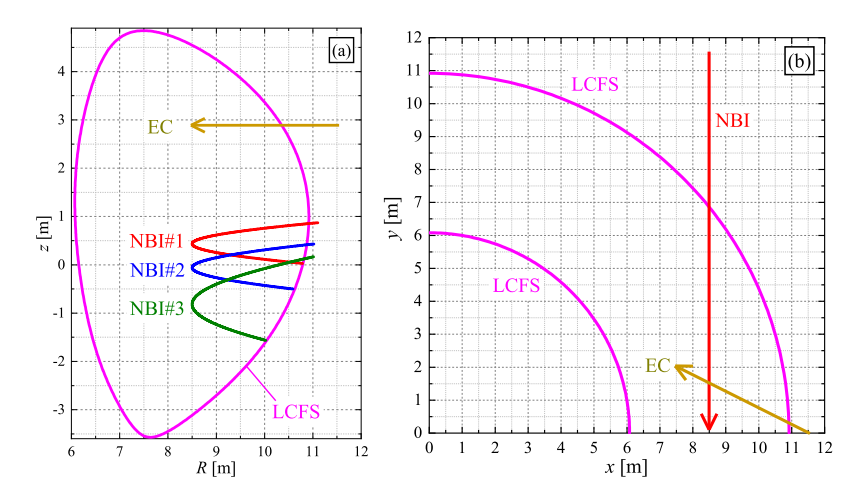


FIG. 1. Last closed flux surface and injection directions of NBI and EC waves in the (a) poloidal plane and (b) horizontal plane of the height of the magnetic axis.

TABLE 1. OBTAINED VALUES OF MAIN PARAMETERS CALCULATED USING TPC AND GOTRESS+WITH THE CDBM, BGB, AND CT MODELS.

Parameters	TPC	CDBM	BgB	CT	Parameters	TPC	CDBM	BgB	CT
$P_{\mathrm{fus}}$ [MW]	1462	1483	1490	1508	$\beta_{ m N}$	3.4	3.67	3.62	3.65
$P_{\mathrm{NBI}}$ [MW]	83.7	75	75	75	$H_{ m H}$	1.31	1.55	1.51	1.53
$P_{\mathrm{EC}}$ [MW]	0	40	40	40	$f_{ m BS}$	0.61	0.61	0.62	0.62
Q	17.5	12.9	12.9	13.1	$f_{ m CD}$	0.39	0.42	0.45	0.43
$f_{ m GW}$	1.2	1.28	1.29	1.29	$Z_{ m eff}$	1.84	2.6	2.6	2.6

normalized by the IPB98(y,2) scaling [29],  $f_{\rm BS}$  is the bootstrap current fraction,  $f_{\rm CD}$  is the externally driven current fraction, and  $Z_{\rm eff}$  is the effective charge. Figure 2 shows the profiles of the (a) electron density,  $n_{\rm e}$ , (b) electron temperature,  $T_{\rm e}$ , (c) ion temperature,  $T_{\rm i}$ , (d) safety factor, q, (e) total current density, (f) bootstrap current density, (g) NBI-driven current density, and (h) EC-driven current density calculated by GOTRESS+ for the cases of using the BgB, CDBM, and CT models. In Fig. 2(a)–(c), the density and temperature profiles assumed in the systems analysis are compared. We determined the central density,  $n_{\rm e0}$ ,  $Z_{\rm eff}$ , i.e., the Ar density fraction,  $P_{\rm NBI}$ , and  $P_{\rm EC}$  so that  $P_{\rm fus}\sim 1.5$  GW,  $f_{\rm NI}\sim 1$ ,  $f_{\rm GW}\sim 1.2$ , and  $P_{\rm sep}\sim 280$  MW are simultaneously obtained in the GOTRESS+ simulation when using the CDBM model. Here,  $f_{\rm NI}=f_{\rm BS}+f_{\rm CD}$  is the non-inductive current drive fraction, and  $P_{\rm sep}\sim 280$  MW corresponds to the allowable heat flux to the divertor [30]. The balance of  $P_{\rm NBI}$  between the three injectors was determined to keep the minimum value of q above one. The EC waves are locally injected to drive the current locally and to form an ITB at  $\rho=0.6$ .

The GOTRESS+ evaluates higher values of  $P_{\rm aux}$ ,  $\beta_{\rm N}$ ,  $H_{\rm H}$ , and  $Z_{\rm eff}$  under the conditions of  $P_{\rm fus}\sim 1.5$  GW,  $f_{\rm NI}\sim 1$ , and  $P_{\rm sep}\sim 280$  MW than the systems analysis, as shown in Table 1. Because the current drive efficiency of NBI is higher than that of EC, and 40 MW of EC is used for forming an ITB, higher  $P_{\rm aux}$  is required to obtain  $f_{\rm NI}\sim 1$  in the GOTRESS+ simulation than that evaluated by the systems analysis. The higher  $Z_{\rm eff}$  is required for  $P_{\rm sep}\sim 280$  MW than  $Z_{\rm eff}$  assumed in the systems analysis, and  $H_{\rm H}$  increases with increasing  $Z_{\rm eff}$ . The higher  $\beta_{\rm N}$  is required for  $P_{\rm fus}\sim 1.5$  GW in the GOTRESS+ simulation than the result of the systems analysis because the systems analysis assumed the temperature profile broader than that calculated by the transport analysis.

The GOTRESS+ simulations using the BgB and CT models are performed with the same parameters as the case of using the CDBM model, other than the transport model, although the optimal conditions might differ depending on the selection of the transport model. Because the BgB and CDBM models include the shear effect, ITBs are formed at the positions where the q profile has local minima, whereas no ITB is observed for the case of the CT model. Three transport models evaluate different temperature and current profiles; however, the main parameters are evaluated to be similar values.

Figure 3 shows the dependence of  $f_{\rm NI}$ ,  $f_{\rm BS}$ , and  $f_{\rm CD}$  on the balance between  $P_{\rm NBI}$  and  $P_{\rm EC}$  when  $P_{\rm aux}=115$  MW for the case of using the CDBM model. Figure 4 shows the dependence of the profiles of the (a) safety factor and (b) ion temperature on the balance between  $P_{\rm NBI}$  and  $P_{\rm EC}$  when  $P_{\rm aux}=115$  MW for the case of using the CDBM model. In JA DEMO, NBI is used for the main current drive source because of its high current drive efficiency, and EC is used for the ITB formation and instability control because of its local current profile controllability. The bootstrap current fraction  $f_{\rm BS}$  increases with

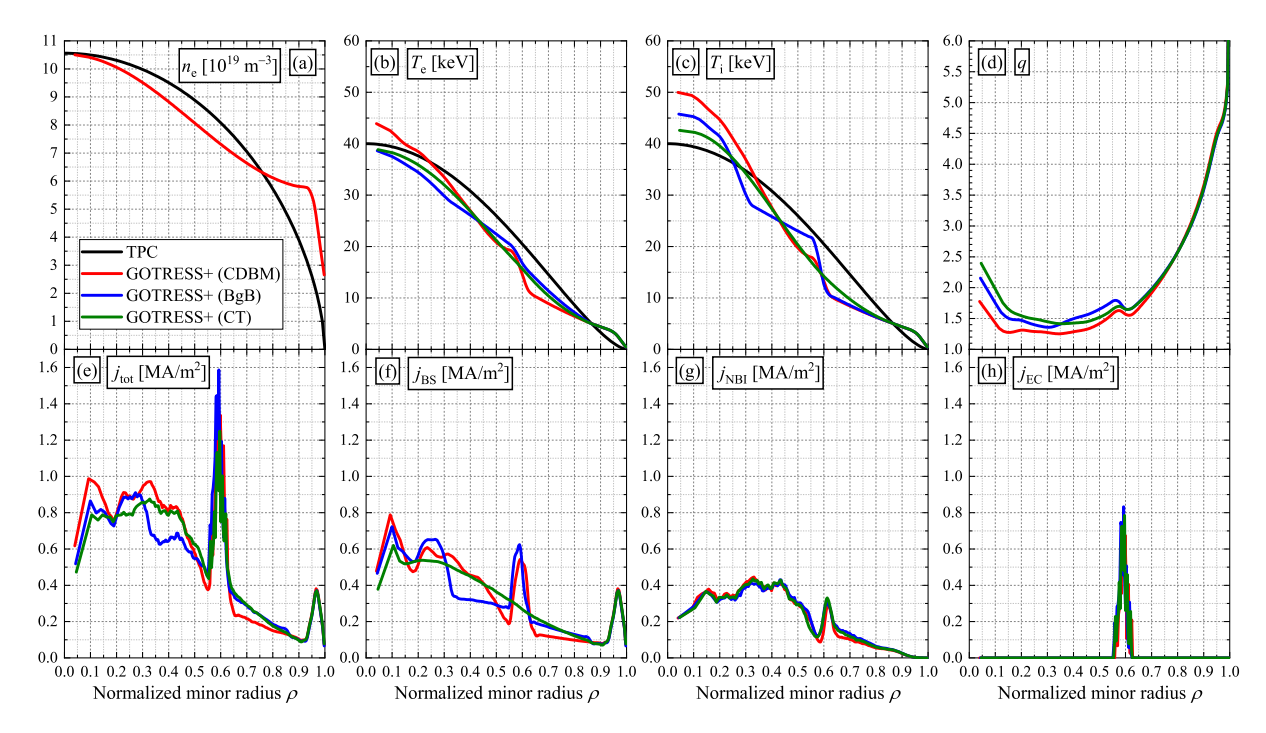


FIG. 2. Profiles of the (a) electron density, (b) electron temperature, (c) ion temperature, (d) safety factor, (e) total current density, (f) bootstrap current density, (g) NBI-driven current density, and (h) EC-driven current density calculated by GOTRESS+ for the cases of using the BgB, CDBM, and CT models.

increasing  $P_{\rm EC}$  because the higher  $P_{\rm EC}$  forms a stronger ITB and increases the temperature inside the ITB. The external current drive fraction  $f_{\rm CD}$  increases with increasing  $P_{\rm EC}$  for  $P_{\rm EC} \leq 20$  MW because the higher temperature increases the current drive efficiency. However, for  $P_{\rm EC} > 20$  MW,  $f_{\rm CD}$  decreases with increasing  $P_{\rm EC}$  because the fraction of  $P_{\rm NBI}$  decreases, resulting in the external current drive efficiency decreasing. Therefore, the optimal balance between  $P_{\rm NBI}$  and  $P_{\rm EC}$  to maximize  $f_{\rm NI}$  exists and is  $P_{\rm EC}/P_{\rm NBI} = 40/75$  for the JA DEMO steady-state operation condition when  $P_{\rm aux} = 115$  MW and using the CDBM model.

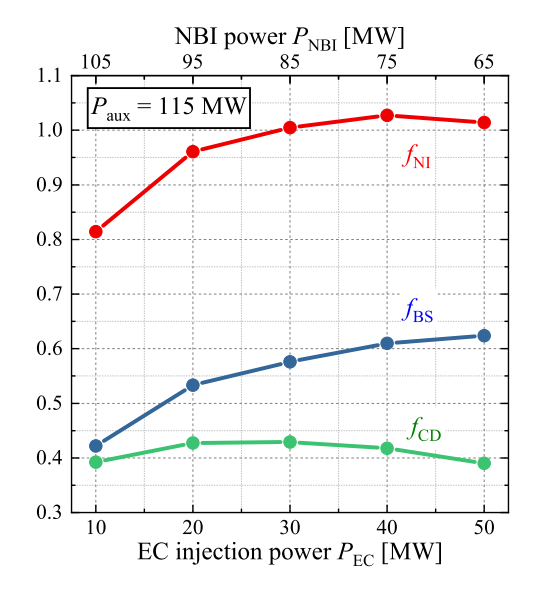


FIG. 3. Dependence of  $f_{\rm NI}$ ,  $f_{\rm BS}$ , and  $f_{\rm CD}$  on the balance between  $P_{\rm NBI}$  and  $P_{\rm EC}$  when  $P_{\rm aux}=115$  MW for the case of using the CDBM model.

Table 2 compares the main parameters for the cases of  $\rho_{\rm EC}=0.5,\,0.6$ , and 0.7 when using the CDBM model and the same parameters as the simulations shown in Fig. 1, other than  $\rho_{\rm EC}$ , where  $\rho_{\rm EC}$  is the location of the EC current drive. Figure 5 shows the dependence of the profiles of the (a) safety factor and (b) ion temperature on  $\rho_{\rm EC}$  for the case of using the CDBM

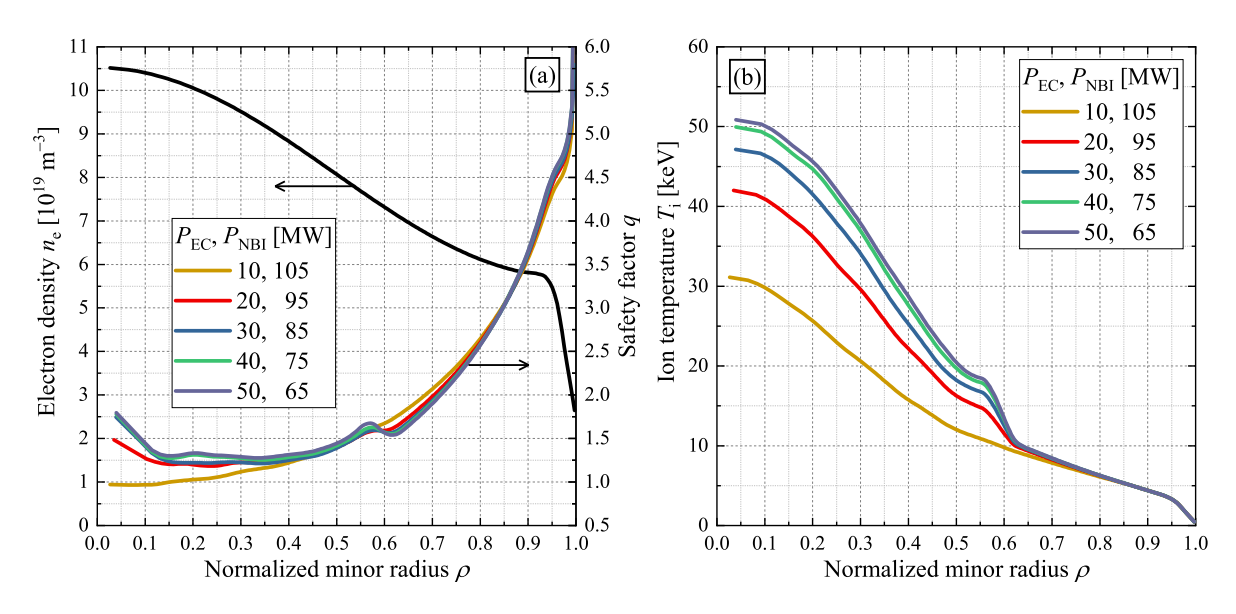


FIG. 4. Dependence of the profiles of the (a) safety factor and (b) ion temperature on the balance between  $P_{\rm NBI}$  and  $P_{\rm EC}$  when  $P_{\rm aux}=115$  MW for the case of using the CDBM model.

model. Depending on the location of the ITB formation,  $P_{\rm fus}$  and  $f_{\rm NI}$  increase with increasing  $\rho_{\rm EC}$ . When  $\rho_{\rm EC}=0.7$ , the q=2 surfaces appear at multiple  $\rho$  positions. The formation of multiple q=2 surfaces should be avoided in terms of magnetohydrodynamic instabilities. Therefore, the optimal value is located in the range  $0.6<\rho_{\rm EC}<0.7$  to increase the plasma performance within the preferred q profile.

TABLE 2. OBTAINED VALUES OF MAIN PARAMETERS FOR THE CASES OF  $\rho_{\rm EC}=0.5,\,0.6,\,{\rm AND}\,0.7$  WHEN USING THE CDBM MODEL.

Parameters	$\rho_{\rm EC} = 0.5$	0.6	0.7	-	Parameters	$\rho_{\rm EC} = 0.5$	0.6	0.7
$P_{\mathrm{fus}}$ [MW]	1311	1483	1882	-	$\beta_{\rm N}$	3.28	3.67	4.77
$P_{\mathrm{NBI}}$ [MW]	75	75	75		$H_{ m H}$	1.46	1.55	1.85
$P_{\mathrm{EC}}$ [MW]	40	40	40		$f_{ m BS}$	0.54	0.61	0.75
Q	11.4	12.9	16.4		$f_{ m CD}$	0.39	0.42	0.47
$f_{ m GW}$	1.26	1.28	1.30		$Z_{ m eff}$	2.6	2.6	2.6

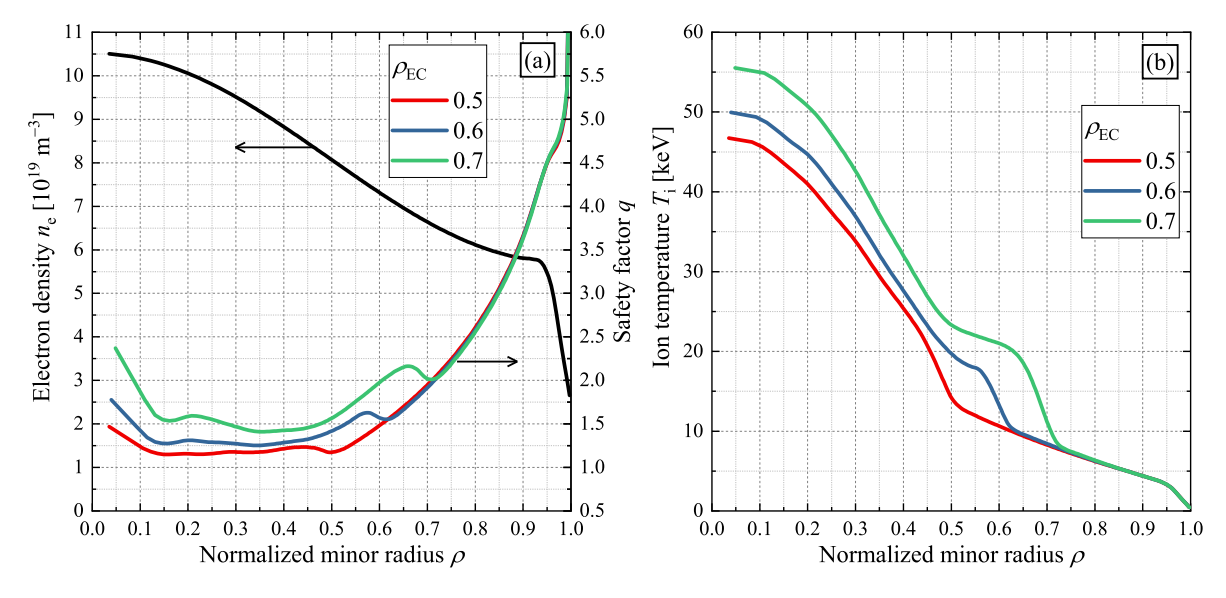


FIG. 5. Dependence of the profiles of the (a) safety factor and (b) ion temperature on  $\rho_{EC}$  for the case of using the CDBM model.

TABLE 3. OBTAINED VALUES OF MAIN PARAMETERS FOR THE CASES OF  $n_{\rm ped}/n_{\rm GW}=0.7,\,0.85,\,$  AND 1.0 WHEN USING THE CDBM MODEL.

Parameters	$n_{\rm ped}/n_{\rm GW} = 0.7$	0.85	1.0	Parameters	$n_{\rm ped}/n_{\rm GW} = 0.7$	0.85	1.0
$n_{\rm e0}/\langle n_{\rm e} \rangle$	1.72	1.51	1.30				
$P_{\mathrm{fus}}$ [MW]	1490	1483	1376	$\beta_{ m N}$	3.67	3.67	3.52
$P_{\mathrm{NBI}}$ [MW]	75	75	75	$H_{ m H}$	1.49	1.55	1.61
$P_{\mathrm{EC}}$ [MW]	40	40	40	$f_{ m BS}$	0.62	0.61	0.56
Q	13.0	12.9	12.5	$f_{ m CD}$	0.45	0.42	0.38
$f_{\rm GW}$	1.27	1.28	1.25	$Z_{ m eff}$	2.6	2.6	2.6

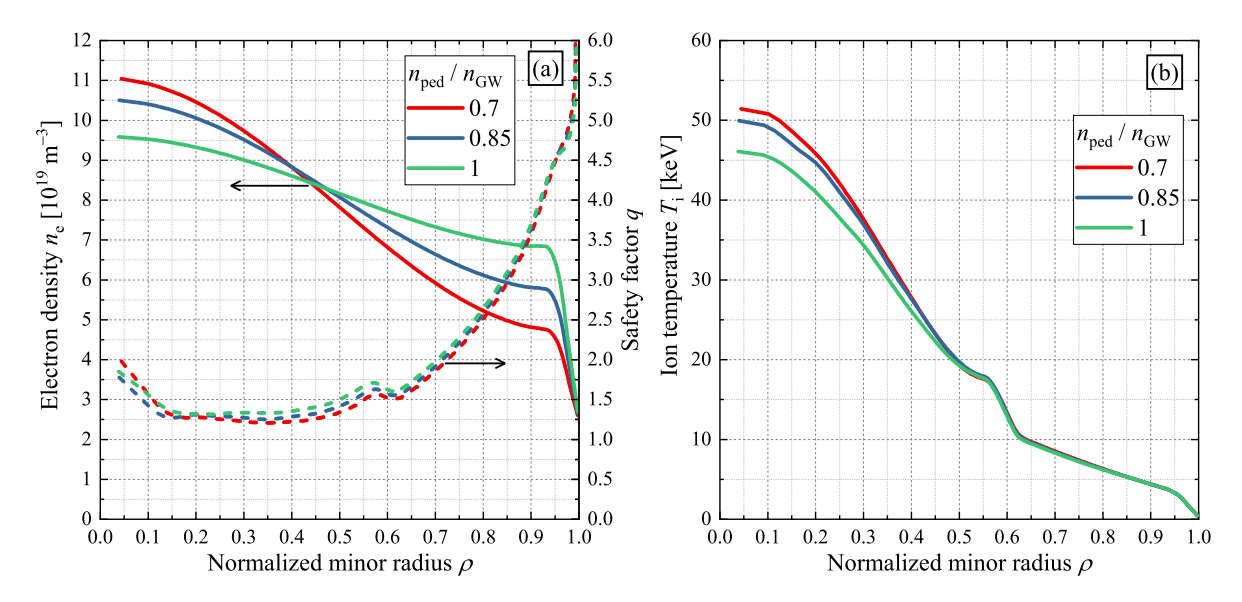


FIG. 6. Dependence of the profiles of the (a) safety factor and (b) ion temperature on the density profile for the case of using the CDBM model.

Table 3 compares the main parameters for the cases of  $n_{\rm ped}/n_{\rm GW}=0.7, 0.85$ , and 1.0 when using the CDBM model and the same parameters as the simulations shown in Fig. 1, other than the electron density profile. Figure 6 shows the dependence of the profiles of the (a) safety factor and (b) ion temperature on the density profile for the case of using the CDBM model. The density peaking factor,  $n_{\rm e0}/\langle n_{\rm e} \rangle$ , is adjusted so that  $f_{\rm GW}$  becomes the same level even for the different pedestal densities, as shown in Fig. 6. When  $f_{\rm GW}$  is the same level, the minimum value of the safety factor and  $H_{\rm H}$  decrease, and  $f_{\rm NI}$  and  $P_{\rm fus}$  increase with increasing the density peaking factor. For  $0.7 \le n_{\rm ped}/n_{\rm GW} \le 1.0$ ,  $P_{\rm EC} = 40$  MW is enough to form ITBs. Although the high density in the edge region is preferable for the divertor operation, the high density peaking factor with the low pedestal density is preferable for the core plasma condition.

# 4. CONCLUSION

We have evaluated the plasma performance in the JA DEMO steady-state operation using GOTRESS+ to address the uncertainties of modelling and assumptions. We have compared the results of the integrated simulations to those of the systems analysis. The GOTRESS+ simulations evaluate higher values of  $P_{\rm aux}$ ,  $\beta_{\rm N}$ ,  $H_{\rm H}$ , and  $Z_{\rm eff}$  to obtain  $P_{\rm fus}\sim 1.5$  GW,  $f_{\rm NI}\sim 1$ , and  $P_{\rm sep}\sim 280$  MW than the systems analysis. We have investigated the plasma performance on the selection of the turbulent transport model, heating and current drive conditions, and density profile. Within the simulation conditions in this study, the plasma performance required for the JA DEMO steady-state operation can be sufficiently obtained.

We have compared the plasma performance simulated using the BgB, CDBM, and CT models, fixing the other simulation conditions. The three models evaluate the different temperature and current profiles; ITBs are formed when using the BgB and CDBM models and are not formed when using the CT model. However, the models predict similar plasma performance, i.e.,  $P_{\rm fus}$ ,  $\beta_{\rm N}$ ,  $H_{\rm H}$ , and  $f_{\rm NI}$ .

In JA DEMO, we suppose to use NBI for the main current drive source because of its high current drive efficiency and EC for the ITB sustainment and instability control because of its local current profile controllability. We have investigated the dependence of  $f_{\rm NI}$  on the balance between  $P_{\rm NBI}$  and  $P_{\rm EC}$  for the case of using the CDBM model. The bootstrap current

increases with increasing  $P_{\rm EC}$  because higher  $P_{\rm EC}$  forms stronger ITBs, resulting in higher temperature. For the same  $P_{\rm aux}$ , with increasing  $P_{\rm EC}$ ,  $f_{\rm CD}$  can increase due to the effect of the temperature increase and can decrease due to the effect of the decrease in the NBI power fraction. Therefore, the optimal balance between  $P_{\rm NBI}$  and  $P_{\rm EC}$  to maximize  $f_{\rm NI}$  exists. For the conditions of the JA DEMO steady-state operation, the optimal balance is approximately  $P_{\rm NBI}=75$  MW and  $P_{\rm EC}=40$  MW when  $P_{\rm aux}=115$  MW.

We have examined the dependence of the plasma performance on the EC current drive location,  $\rho_{\rm EC}$ , i.e., ITB foot position, for the case of using the CDBM model. When the conditions other than  $\rho_{\rm EC}$  are fixed,  $P_{\rm fus}$  and  $f_{\rm NI}$  increase with increasing  $\rho_{\rm EC}$  in the range of  $0.5 \le \rho_{\rm EC} \le 0.7$ . The q=2 surfaces appear at the multiple  $\rho$  position when  $\rho_{\rm EC} \gtrsim 0.7$  for the case of  $P_{\rm EC}=40$  MW; the formation of multiple q=2 surfaces should be avoided in terms of the magnetohydrodynamic stability. The optimal location of the EC current drive to increase the plasma performance while avoiding the formation of multiple q=2 surfaces is found within the range of  $0.6 < \rho_{\rm EC} < 0.7$ .

We have investigated the dependence of the plasma performance on the density peaking factor, changing the central and pedestal density and fixing  $f_{\rm GW}$ , for the case of using the CDBM model. When the conditions other than the density profile are fixed, the minimum value of the safety factor and  $H_{\rm H}$  decrease, and  $f_{\rm NI}$  and  $P_{\rm fus}$  increase with increasing the density peaking factor. The EC injection power of 40 MW is enough to form ITBs for  $0.7 \le n_{\rm ped}/n_{\rm GW} \le 1.0$ . Although the high density in the edge region is preferable for the divertor operation, the high density peaking factor with the low pedestal density is preferable for the core plasma condition.

#### ACKNOWLEDGEMENTS

This work was carried out within the framework of the Broader Approach DEMO Design Activity.

## REFERENCES

- [1] TOBITA, K., et al., Overview of the DEMO conceptual design activity in Japan, Fusion Eng. Des. 136 (2018) 1024.
- [2] SAKAMOTO, Y., et al., Development of physics and engineering designs for Japan's DEMO concept, 27th IAEA Fusion Energy Conf. (2018) FIP/3-2.
- [3] SUGIYAMA, S., et al., A study on ohmic plasma initiation for JA DEMO, Fusion Eng. Des. 172 (2021) 112779.
- [4] WAKATSUKI, T., et al., Reduction of poloidal magnetic flux consumption during plasma current ramp-up in DEMO relevant plasma regimes, Nucl. Fusion **57** (2017) 016015.
- [5] SUGIYAMA, S., et al., Parameter study of L–H transition for plasma operation scenario development in JA DEMO, Fusion Eng. Des. **187** (2023) 113369.
- [6] TOKUNAGA, S., et al., Conceptual design study of pellet fueling system for DEMO, Fusion Eng. Des. 123 (2017) 620.
- [7] SUGIYAMA, S., et al., Development of pulsed plasma operation scenario and required conditions in JA DEMO, Nucl. Fusion **64** (2024) 076014.
- [8] SICCINIO, M., et al., Impact of the plasma operation on the technical requirements in EU-DEMO, Fusion Eng. Des. **179** (2022) 113123.
- [9] MAVIGLIA, F., et al., Integrated design strategy for EU-DEMO first wall protection from plasma transients, Fusion Eng. Des. **177** (2022) 113067.
- [10] SICCINIO, M., et al., DEMO physics challenges beyond ITER, Fusion Eng. Des. 156 (2020) 111603.
- [11] SICCINIO, M., et al., Development of the plasma scenario for EU-DEMO: Status and plans, Fusion Eng. Des. 176 (2022) 113047.
- [12] POLEVOI, A. R., et al., Assessment of operational space for long-pulse scenarios in ITER, Nucl. Fusion **55** (2015) 063019.
- [13] KIM, S. H., et al., Investigation of key parameters for the development of reliable ITER baseline operation scenarios using CORSICA, Nucl. Fusion **58** (2018) 056013.
- [14] KIM, S. H., et al., A study of the heating and current drive options and confinement requirements to access steady-state plasmas at  $Q \sim 5$  in ITER and associated operational scenario development, Nucl. Fusion **61** (2021) 076004.

- [15] SICCINIO, M., et al., Development of a plasma scenario for the EU-DEMO tokamak reactor, 29th IAEA Fusion Energy Conf. (2023) 1661.
- [16] HONDA, M., et al., Development of a novel integrated model GOTRESS+ for predictions and assessment of JT-60SA operation scenarios including the pedestal, Nucl. Fusion **61** (2021) 116029.
- [17] TANI, K., et al., Numerical analysis of 2D MHD equilibrium with non-inductive plasma current in tokamaks, J. Comput. Phys. **98** (1992) 332.
- [18] HAMAMATSU, K., FUKUYAMA, A., Controllability of driven current profile in ECCD on ITER, Fusion Eng. Des. **53** (2001) 53.
- [19] HONDA, M., NARITA, E., Machine-learning assisted steady-state profile predictions using global optimization techniques, Phys. Plasmas **26** (2019) 102307.
- [20] TANI, K., et al., Effect of toroidal field ripple on fast ion behavior in a tokamak, J. Phys. Soc. Jpn. 50 (1981) 1726.
- [21] ERBA, M., et al., Validation of a new mixed Bohm/gyro-Bohm model for electron and ion heat transport against the ITER, Tore Supra and START database discharges, Nucl. Fusion **38** (1998) 1013.
- [22] GARCIA, J., et al., Physics comparison and modelling of the JET and JT-60U core and edge: towards JT-60SA predictions, Nucl. Fusion **54** (2014) 093010.
- [23] HAYASHI, N., et al., Transport modelling of JT-60U and JET plasmas with internal transport barriers towards prediction of JT-60SA high-beta steady-state scenario, Nucl. Fusion **57** (2017) 126037.
- [24] FUKUYAMA, A., et al., Transport simulation on L-mode and improved confinement associated with current profile modification, Plasma Phys. Control. Fusion 37 (1995) 611.
- [25] HONDA, M., FUKUYAMA, A., Comparison of turbulent transport models of L- and H-mode plasmas, Nucl. Fusion **46** (2006) 580.
- [26] JARDIN, S. C., et al., TSC simulation of ohmic discharges in TFTR, Nucl. Fusion 33 (1993) 371.
- [27] SNYDER, P. B., et al., Development and validation of a predictive model for the pedestal height, Phys. Plasmas 16 (2009) 056118.
- [28] AIBA, N., et al., Extension of the Newcomb equation into the vacuum for the stability analysis of tokamak edge plasmas, Comput. Phys. Commun. **175** (2006) 269.
- [29] ITER Physics Expert Group on Confinement and Transport, et al., Chapter 2: Plasma confinement and transport, Nucl. Fusion **39** (1999) 2175.
- [30] ASAKURA, N., et al., Simulation studies of divertor detachment and critical power exhaust parameters for Japanese DEMO design, Nucl. Mater. Energy **26** (2021) 100864.